New methodologies for on-site characterization of line-focus solar collectors' fields

Identification of autonomous robots and UAV/IAV and completion of systems design

STAGE-STE Project	
Scientific and Technological Alliance for Guaranteeing the European Excellence in Concentrating Solar Thermal Energy	
Grant agreement number:	609837
Start date of project:	01/02/2014
Duration of project:	48 months
WP11 – Task11.2.2	MS41
Due date:	January/2016
Submitted	February/2016
File name:	WP11 MS41 STAGE-STE_Deliverable
Partner responsible	ENEA / Cranfield
Person responsible	Marco Montecchi / Paul Comley
Author(s):	Marco Montecchi (ENEA), Paul Comley (Cranfield), Loreto Susperregui (TEKNIKER), Fabienne Sallaberry (CENER)
Dissemination Level	*(as indicated in DoW)*

List of content

Executive Summary

This deliverable, MS41 - Identification of autonomous robots and UAV/IAV and completion of systems design, is part of the *WP11 Linear focusing STE activities* contained within *task 11.2. New methodologies for dynamic testing and predictive maintenance of large solar fields*, and *subtask 11.2.2 New methodologies for on-site characterization of line-focus solar collectors' fields*.

The report outlines the possible integration of remote sensors in both terrestrial and aerial vehicles for fast characterization of line-focus solar fields one of the purposes of the ongoing project STAGE-STE project. Possible tasks of Unmanned Aerial Vehicle (UAV) and Intelligent Autonomous Vehicle (IAV) are covered together with the minimal system requirements.

1 Introduction

The increasing number of commercial solar thermal power plants is demanding the definition of predictive maintenance procedures to improve reliability and the number of operating hours. The most important inspections on solar fields are:

1. Optical and thermal analysis of linear solar receivers on-site;

2. Optical and geometrical analysis of line-focus reflectors on-site;

3. Status testing of the heat transfer fluid;

4. Testing of other components of the solar fields.

The integration of remote sensors in both terrestrial and aerial vehicles for fast characterization of line-focus solar fields is one of the purposes of the ongoing project STAGE-STE. The present document reports on the possible tasks Unmanned Aerial Vehicle (UAV) and Intelligent Autonomous Vehicle (IAV) can do, and the minimal system requirement of the robot.

Although the term IAV was used in the documents illustrating the project aim, in the following it is replaced by Unmanned Ground Robot (UGR): as matter of fact the term intelligent implies the having of logic and understanding abilities which are not really necessary for dealing ground inspection of solar fields. Much more simply the most important feature for these machines is the autonomous working with reasonably short measuring-time

2 Applications for UAV and UGR

STAGE-STE partners are studying and developing methods related to the topic of this document. They are listed and briefly described in the following

2.1 Geometrical measurements by close-range photogrammetry

Close-range photogrammetry is one of the most diffuse techniques used in CSP for the geometrical characterisation of structures and components. The main components are a high resolution camera and a set of targets. The technique requires that a pattern of targets are placed on the important areas of the object. Targets should be high contrast black and white, or retro reflective. This improves both the point recognition and the accuracy of the algorithms used to find the central points of each target. The targets may be constructed of a coded ring or sequence of shapes surrounding a central disk. These coded rings enable automation of the photogrammetry point matching. The target placement is currently manual, requiring direct access to all the required points and may take significant time depending on the required coverage. Ideally targets should be easily applied and detached, leaving no adhesive residue and may be presented as sheets to lessen the application time. Following the target application, several photographs must be taken, from different angles, using a high quality, low distortion camera. This is typically a DSLR camera with high resolution, large sensor and a fixed focus lens. The photographs should be taken from different points of view surrounding the object, covering as many angles as are practical. The camera and lens system must be calibrated to reduce the

distortion of the images. This may be done away from the object, by using calibration sheets, or alternatively may be done using the actual photographs taken of the object. This method is preferred, as it replicates the exact lens settings and object that is under measurement. To aid in this calibration the camera should be rolled around the optical axis for some of the photographs. The lens parameters obtained are then considered in the image processing. Most photogrammetry software allows the use of automatic target matching utilising the coded targets, but some point selection and corrects may be required. It is possible to fully automate the image analysis and processing. A scale must be introduced into the model, which may be formed from a known scale bar introduced into the photographs, with photogrammetry targets attached.

Advantages of the technique are low cost, and high accuracy (typically some mm for objects sizing tens of metres and less than 0.1mm for facet sized objects). Disadvantages are the need to apply targets to the surfaces, the semi-manual image processing, and the low spatial density of the measured points.

Photogrammetry can be used to measure the collector geometry. Because collectors are not perfectly rigid, their shape is generally affected by the gravity, depending on their orientation. Therefore aerial photogrammetry is a very important tool because allows the collector geometry to be determined in working orientations along its daily trajectory.

Cranfield has previously developed a photogrammetry technique for measuring a range of solar collectors, including parabolic trough facets and modules. This technique has been validated to better than 100 microns against a tactile coordinate measuring machine [1], itself traceably accurate to less than 10 microns over the size of a typical facet. The photogrammetry technique currently involves a handheld camera, and will be extended to operate with a UAV mounted camera. Handheld photogrammetry measurements have been performed on EuroTrough collectors, both at the individual facet and whole module scales. When measuring whole modules it is necessary to use larger diameter photogrammetry targets, due to the increased distance required from the mirror and the wider field-of-view.

Measurements at CIEMAT-PSA of whole modules used 9 targets per facet each with a central disk size of 30 mm. Using only 9 targets decreases the time required to attach and remove the targets and so is more suitable than covering whole facets when investigating a number of modules.

There is a general requirement for photogrammetry that the target should have an on-sensor size of greater than 5 to 10 pixels for proper identification. The 30 mm target size is sufficient for correct identification of both the central disk and the surrounding coded target ring at a distance of up to 15 m between camera and target, at angles up to 45 degrees. For capturing more than one trough, it may be necessary to use larger targets; however this could be calculated as required by using the field of view and resolution of the camera with the size of the required area for capture. In the case of the EuroTrough measurements, 9 targets were sufficient to identify millimetre scale errors both in module shape and facet alignment.

Measurements at CENER for the characterization of the geometry of mirrors shape accuracy use a high resolution camera (Camera Canon EOS 5d Mark II (lenses Canon EF 24 mm and Canon EF 100-400 mm) some targets and a specialized post-processing specific software (PhotoModeler 2015) for the analysis of the data acquired. A posterior data processing with an own software tool determines the geometry of the concentration system mirrors and using ray-tracing (Tonatiuh, open access software) allows to determine the amount of energy that will reach the solar receiver tube as a function of the reconstructed shape of the collector surfaces and their mirror quality, and compares it with the amount of energy that will reach an ideal solar receiver tube from an ideal mirror collector under the same circumstances.

2.2 Vacuum status of linear receivers

The thermal insulation of the evacuated receiver strongly depends on the vacuum state; when lost, part of the absorbed solar energy is dissipated by thermal convection, reducing the receiver effectiveness. Because large parabolic trough/ linear-Fresnel solar fields consist of tens of thousands of receiver tubes, a fast non-contact method for checking the receiver vacuum state is highly desirable.

One method of interest is the analysis of infrared images acquired with commercial thermo-cameras: except for a few narrow “windows”, glass is not transparent in IR, thus the thermo-camera detects the temperature of the outer surface of the glass enveloping the absorber. When the vacuum is lost, the outer temperature is higher by an order of magnitude with respect to the good working ones. In other words, the defective tubes can be easily localized by comparison: in the IR image defective (good working) appear as Ne-lamps switched on (switched-off).

The method for the inspection of the receiver tubes combines the thermography measurements of the glass surface temperature camera on a moving vehicle with a detailed heat loss model. Comparing the estimations of the heat loss model and the glass temperature measurements gives useful information to evaluate the vacuum state and the heat loss of the receiver tubes. Glass temperature is directly related to heat loss due to the outer heat transfer model, whereas it informs of the vacuum state due to the inner heat transfer model.

The inspection system requires accurate measurements of some parameters of the plant to reliably typify the receiver tubes. In this sense, environmental conditions ought to be steady in order to guarantee that the measured ambient conditions are the real conditions at which the rest of parameters are evaluated.

The thermography measurement technique is based on the Wien displacement law, the maximum radiation moves towards shorter wavelength as the target temperature rises (λ_{maxT} = constant). The object target is the receiver tube glass cover at a temperature around 40ºC, the radiation emitted will have a maximum wavelength λ_{max} is 2898/T = 2898/(273.15+40ºD) = 9.25 µm which is between the spectral range of the IR camera 7-14 µm.

As it is shown in Fig. 1, the radiation from the tube reaches the IR camera via the atmosphere. The signal is converted to value of superficial temperature of the glass tube assuming a value of the glass emittance ε.

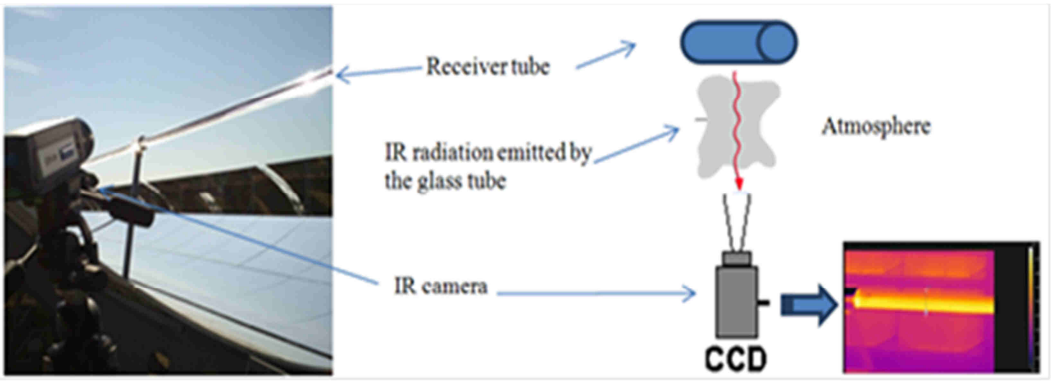

Fig. 1 Scheme of Thermography theory

The main components of the system should be: IR thermal camera, computer, orientation and stabilization device, monitoring controllers, image processing and software to determine the surface temperature. The key component of the developed system is the IR thermography camera. The thermal IR camera should meet important requirements such as: resolution, spectral range, view angle, IR video recording, acquisition frequency, auto-focus, etc.

The MAINBOT FP7 project has developed service robots based applications to autonomously execute inspection tasks in extensive industrial plants in equipment that is arranged horizontally (using ground robots). Among the activities performed by the robots MAINBOT proposes the ground robot patrolling at night and using thermography inspection to identify loss of vacuum problems. To the success of the operation, the thermography camera had to be maintained at a proper orientation and distance with respect the object to be inspected, in order to maintain the target object in the field of view of the camera. Several tests were successfully carried out.

The inspection system developed by CENER performs measurements of the glass surface temperature of the receiver tubes on a moving vehicle in a fast thermographic process. The measurement method consists of a video recording IR images along the half-loops. The vehicle goes parallel to the direction of the half-loop at a maximum distance of 4-5 m and approximately at 15-20 km/h in such way that the receiver tube is always central on the image. Software has been developed to calculate the temperature of each glass tube from videos of IR thermography images. Depending on the temperature measurement value, the software classifies tubes in three different states corresponding to three colours: green (ok), orange (regular) and red (not ok).

2.3 Check of reflectance, soiling, and integrity of mirrors

Specular reflectance of solar collectors is a critical factor in determining the energy output of the system. Any loss in reflectance, for example caused by soiling, corrosion or breakages, will have a significant and immediate effect. It is therefore important to be able to monitor the quality of both the front and rear mirror surfaces. The soiling will occur on the front mirror surface and must be removed during the ongoing regular maintenance by washing. The monitoring of the soiling will inform the frequency of washing required, which must be carefully controlled so as to ensure a high cleanliness is maintained, but without using excess water or chemicals.

Reflectance loss will also occur due to defects such as corrosion spots on the rear surface of the mirror. These will cause parts of the mirror to no longer reflect the light, and should be identified so can they can be treated to prevent spot growth and further reflectance loss.

Specular reflectance is a key measure of the soiling of a mirror. This can be measured using portable reflectometers, for example the D&S 15R or the Abengoa Condor. Such reflectometers are handheld and so would be suitable for use by an autonomous ground based vehicle. In the case of the D&S 15R careful alignment must be done when taking measurements due to the low acceptance angle of the instrument, typically less than 50 mrad. However, the Condor has a much wider acceptance aperture of 400 mrad, and so does not require alignment for measurements. The 15R measures a single wavelength at 660 nm, the condor measures 6 wavelengths between 435 nm and 1050 nm. Once calibrated, the reflectometer will capture the reflectance of the mirror and this can be done quickly over many facets as required. The results can be stored in the device for later analysis.

A visual inspection may be carried out by a video camera, which is focussed at the reflector surfaces. Any defects, for example from dirt or corrosion of the back surface, can be then identified and subsequently investigated.

Reflectivity measurement has been performed using the manual reflectometer (the most widely used in this kind of facilities) integrated in the ground robot in MAINBOT project. The project has tested the ground robot placing the same reflectometer on the points of the SCE that TORRESOL uses as reference and recording the acquired values. The key problem (positioning of the sensor on top of a fragile mirror surface) has been validated. The platform navigates up to the mirror to be inspected, the reflectometer tool-holder is positioned parallel to the mirror and the approach manoeuvre is performed until the sensor touches the mirror. The signals provided by the 3 ultrasound sensors in the tool-holder are used for trajectory control. A real implementation will demand a different approach to include the reading of the sensor values to close the positioning loop and a procedure for periodic re-calibration of the sensor.

2.4 Optical alignment of receiver-reflector for parabolic-trough and linear-Fresnel modules

In field the right question one should ask, in front of a parabolic-trough / linear-Fresnel module, is not “how good is the facet shape?”, but “how good is the mutual optical alignment reflector-receiver?”.

ENEA have developed a composite instrument family based on the Visual Inspection System methodology: the VIS concept is the observation, in the near field, from a number of different points of view, one or more objects put-in or close-to the focus of the solar reflector [2,3]. The VISfield is the ground-instrument for measurements in solar-field. It is composed by a camera mounted on a motorized rail installed on a cargo trailer. The instrument has to be positioned centrally, about 7 m away from the module under investigation; the module is oriented towards the horizon; the motorized rail is set vertically, i.e. parallel to the canonical abscissa of the parabola; the camera is oriented towards the module; the camera height is tuned with the true abscissa value by means of a laser optical level. The joint use of camera and optical level allows a check also of the offset angle of the module alignment, as well as the rightness of the receiver unit alignment along the plane made by the joint-pivots and the horizontal aiming.

Fig. 2 shows the optical scheme of the VISfield; here the Sun is only hypothetical, and is drawn to explain the instrument working. Briefly, the observer (the camera) in V sees the image of the receiver spread around the point P with same abscissa xV of the camera. Misalignment of facet and/or receiver cause(s) the shift of the receiver-image, which borders are expected to appear in x_{min} and x_{max} in the case of perfect alignment. On the other hand, according to the Helmholtz's theorem about the reversibility of the light path, the hypothetical solar spot hitting the receiver is always viewed between xs_{min} and xs_{max}. Therefore the intercept factor is given by the fraction of the solar-spot-image covered by receiver-image.

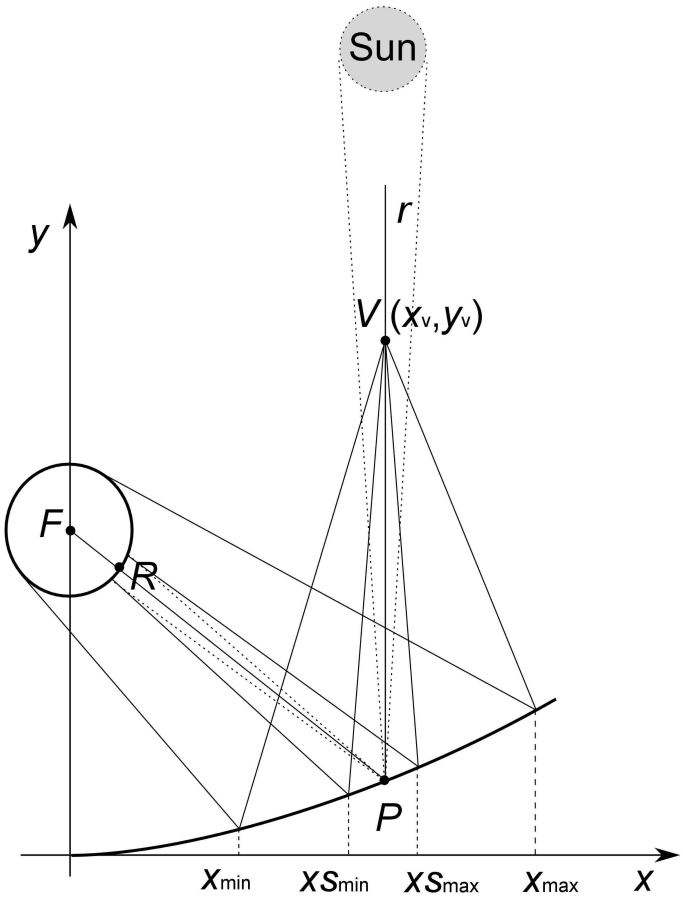

Fig. 2. Optical scheme of the VISfield.

The intercept factor map of the module is obtained by processing some hundreds of images captured at different abscissa values in the aperture range of the parabola. The instrument also gives detailed information on how improve the alignment of each facet (canting). Finally the intercept-factor map of each facet represents its final quality check.

VISfield is a powerful instrument, that can be systematically used during the solar-field construction, but due to the measuring time of about 1 module/hour, the instrument can not be used for the periodic check of the whole solar field. At that purposes ENEA is developing the aerial version of the instrument, named VISfly: it essentially consists of a UAV equipped with a high frame rate camera. VISfly is less accurate than VISfield, but the short measurement time (less than 1 module/minute) makes it suitable for the periodical checking of large solar fields

3 System outlines for solar-field diagnostics

3.1 UAV

A UAV is a powered, aerial vehicle that does not carry a human operator, uses aerodynamic forces to provide vehicle lift, can fly autonomously or be piloted remotely, can be expendable or recoverable, and can carry a lethal or nonlethal payload. Beyond the aircraft itself, some other components are essential, such as the ground control station and a data link for transmitting all or part of the acquired data to the ground.

The size of UAV's ranges from tens of centimetres up to several metres, and the weight from hundreds of grams up to kilos.

Currently the development of UAV is very fast, with an increased use in civil applications. At the same time their cost is constantly reducing, making UAV more and more attractive. As an example, recently the market offers high quality brush-less electric motors besides the conventional combustion engines. At the same time, the development of compact high capacity electric batteries, as well as of electronic devices, make more convenient electric UAVs, which are today the most popular for both hobby and professional applications. The use of fuel cells is just experimental, but the results are very promising for extending the flight range.

Electric motors are the most suitable choice for any solar-field diagnostics based on image acquisition, because now their technology is mature with low levels of vibration aiding the acquisition of high sharpness images.

Because the UAV stability is limited by the air turbulence, the camera should not rigidly hang to the UAV, but always by means a gyro-stabilised gimbal equipped with anti-vibration suspensions (Fig. 3)

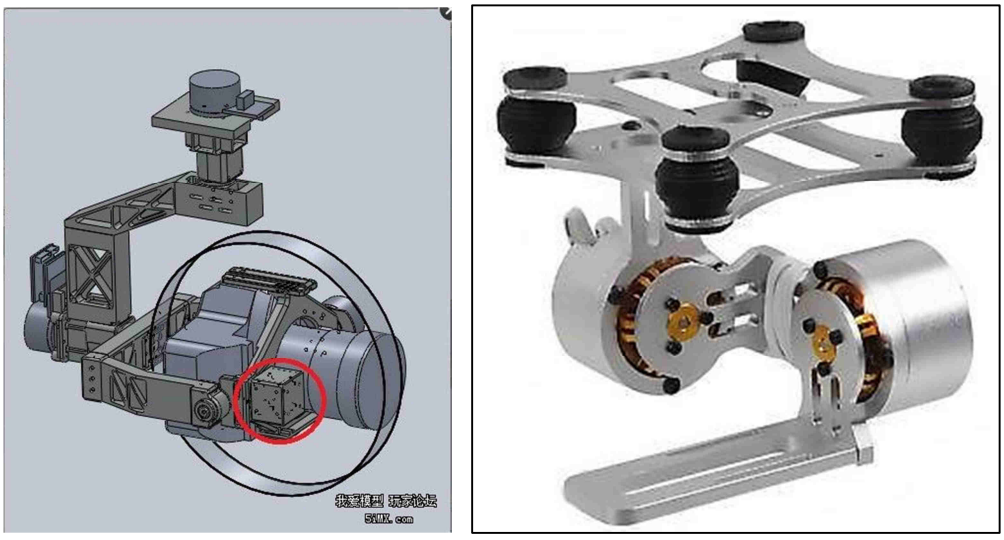

Fig. 3. Sketch and example of brush-less gimbal.

Basically UAVs are categorized in three groups:

- Helicopter / Multicopter
- Convertiplane
- Fixed-wing

Helicopter and multicopter have vertical take-off and landing, and can maintain a stable static position. With respect to fixed-wing the draw-backs are higher fuel consumption and no gliding flight capability. Convertiplanes sum the advantages of the other two, but take-off and (especially) landing are more critical due to the re-action of the moved air back on the wings from the ground.

In respect of solar diagnostics the most suitable UAV class is certainly the multicopter, which is also the most economical compared to all the others. The number of helices should be chosen considering the payload, i.e. the weight of the camera selected for the specific solar diagnostic. As a general rule, the higher the number of motors / helices, the higher the safety factor. Recently more powerful motors have come onto the market, which allow a reduction in weight and number of motors needed for a given load capacity, hence currently four or six helices are the most convenient solutions.

In any case the bottleneck of the multicopter is the firmware which adjusts the boost of each one of the motors for compensating in real time the attitude of the UAV taking into account the inclinometer data. There are several commercial firmware options, but generally specialist UAV operators currently use custom built versions.

Generally UAVs are also equipped with GPS. The flight can be planned by setting a number of waypoints, the coordinates of which have to be entered in the software for the UAV flight automatic control: after the take-off, the UAV will travel to reach the first waypoint; when reached, the UAV will fly towards the next; finally it will land at the starting point or some other selected point.

When image-acquisition is the main target of the flight, the ground operator should be able to monitor what the camera is seeing, and he should be able to adjust the camera-aiming and/or the UAV attitude. In the case of a high resolution camera, just a downgraded image should be transmitted to the ground.

Figure 4 - DJI Inspire UAV

Figure 5 - HexCam hexacopter

Cranfield is currently working with a UK company *HexCam*, to investigate and specify a suitable UAV platform. The tests aim to establish a suitable combination of UAV configuration, with camera mount and resolution as modelling dynamic and vibratory effects would be very time consuming and expensive. Two systems under initial evaluation are the DJI Inspire quadcopter with built in stabilised 12 Mpixel camera with 1/2.3 inch sensor and fixed optics (Figure 4), and a custom built hexacopter

with a gimbal mounted Sony NEX-7 24 Mpixel camera with an APS-C size sensor and fixed zoom lens (Figure 5).

Figure 6 shows close-ups of the acquired images, it is clear that the larger sensor and higher quality optics of the heavier NEX-7 camera mounted on the custom hexacopter produced significantly higher quality images and thus a more reliable and more accurate photogrammetry measurements than could be obtained using the small sensor built-in camera on the lower capacity DJI Inspire.

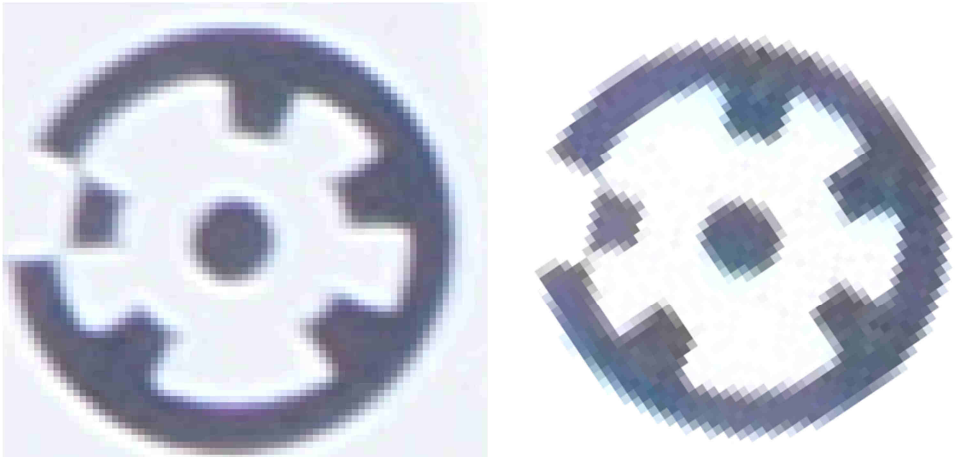

Figure 6 - Close-up of photogrammetry targets with NEX-7 (l) and DJI Inspire (r)

Mounting higher resolution cameras and stabilised gimbals leads to a significantly increased weight requirement, which is likely to result in requiring UAVs with greater lifting power, increasing the cost and decreasing the flight time available. The use of a relatively light-weight, mirrorless cameras with a similar specification of DSLR camera quality would maintain the photogrammetry accuracy whilst keeping the weight low. For example, the Cranfield Canon 600d with lens has a total weight of 770g and measures approximately 130x100x150mm. A Sony a6000 has been chosen, as with a lens this can weigh as little as 420g and measures only 120x67x45mm. This weight and size saving then requires a smaller and lighter gimbal, so the weight difference becomes more significant. The gimbal chosen is the “EZ-Gimbal Pro With A Twist” from Grouse House Technologies (Figure 7). This gimbal is primarily constructed of carbon fibre for weight saving and strength and has a camera roll feature. This enables the quick change of camera angle between landscape and portrait without requiring a rebalance of the system. This gimbal will be attached to a hexacopter frame. The system as a whole is targeted to be below 7kg, a UK regulatory limit set by the CAA below which the flight restrictions are significantly reduced. This lower weight will also increase the flight time, the HexCam hexacopter achieved 15-20 minutes per set of batteries. Ultimately measurement time can be extended with additional high capacity batteries and may improve as battery, drone and camera technology advances. Additional UAV capabilities should include a GPS system that allows the recording of waypoints and the possibility of automatic camera pointing. This would increase the autonomy of the UAV system and allow faster and more repeatable measurements to be taken. There are currently some limitations on the accuracy of GPS systems, typically around 1-2m, which would reduce the waypoint repeatability. However, the use of a Real-Time Kinetic (RTK) system, where a base station is used in addition to the UAV GPS can increase the GPS accuracy to the centimetre level. While it is unlikely that the UAV will be able to repeat a position to this level, due to variations in wind speeds and stability, the added GPS accuracy should improve its positioning. Additionally a UAV should be able to provide a long range downlink of the camera view and allow full control over the camera settings remotely. The hexacopter will have the DJI A2 controller, including GPS, and a DJI Lightbridge downlink.

Figure 7 - EZ-Gimbal Pro With A Twist

Any activity with UAVs should follow the specific regulations given by each country's National Flight Agency. Currently due to the quick diffusion of UAVs, some European countries are reviewing their regulations and so additional constraints may become a consideration in the initial selection criteria.

3.2 UGR

Automating inspection activities using robots has been a challenge for years. One of the requirements for this project is to use robots to apply diagnostic tools. There are many design approaches for a broad range of applications and environments, below is an overview of robots used with different NDT inspection technologies.

Although there is currently a wide range of NDT, visual inspection techniques (and associated aids, such as hand-held devices, endoscopes, borescopes) play an important role in assessing system condition. There are even commercial solutions that offer robotized visual inspection as shown in Figure *8*.

Figure 8: Left, visual inspection with commercial Borescope (from Gradient Lens Corp), right, robotic visual inspection system (rovion®).

Radiography testing [4] is done by exposing a target object to penetrating radiation to inspect elements for failures. The radiation passes through the object and projects the shadow image of the

object onto a film or other media. The resulting image (as most people have seen in medical radiographs) shows the internal aspect of the inspected element. Possible imperfections are indicated as density changes in the film.

Commercial solutions offer a full range of industrial radiographic equipment. Some provide mobile digital radiography solutions that can be applied for pipe corrosion inspection, wall thickness measurement and weld quality [5].

Figure 9: JME crawler for panoramic radiographs [5]

Ultrasonic testing [4] uses transmission of high-frequency sound waves to detect imperfections. Ultrasonic testing analyses the reflected waves (pulse-echo) or the transmitted waves (through-transmission). Automated systems typically consist of an immersion tank, scanning system, and recording system of the scan. Some robotic solutions can be found such as SAUL [5] that integrates robotics and ultrasound scanning for aeronautical composite inspection, and ultrasonic inspection robot that automatically search for damage, corrosion, and cracks in pipelines [7] as shown in Figure 10.

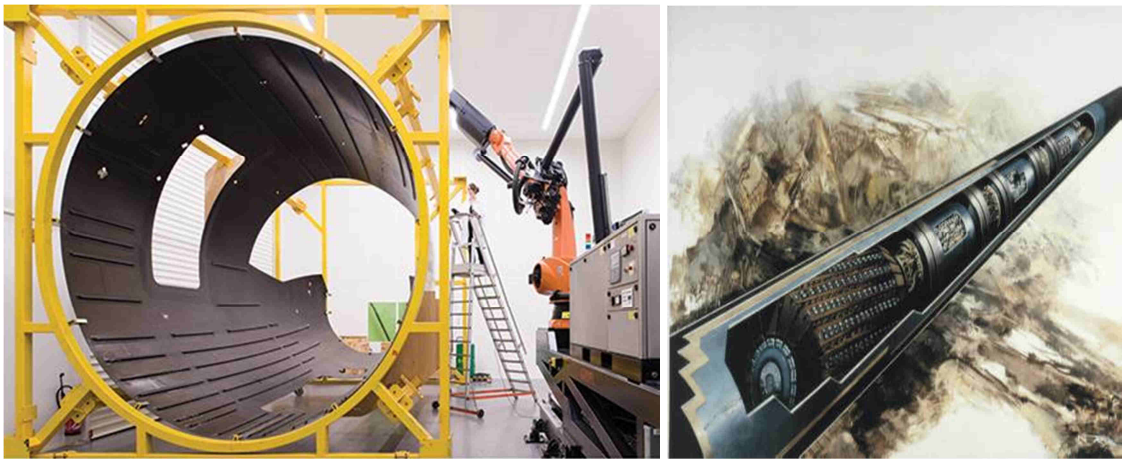

Figure 10: Robotic ultrasound solutions for composite and pipe inspection

3.2.1 Robot types

There is a requirement for both elevated and ground based inspection in the solar field. Hence this section describes a range of existing robots technologies being considered, the first group with climbing ability the second ground based.

3.2.1.1 Climbing inspection robots

The following section gives a short overview about existing climbing robots for different inspection and maintenance tasks. The overview is structured by the different climbing methods. Main application fields for operating climbing robots are power plant, power line and bridge inspections.

Climbing robots to move on cables for inspection and/or repair of bridges and power lines, see Figure 11.

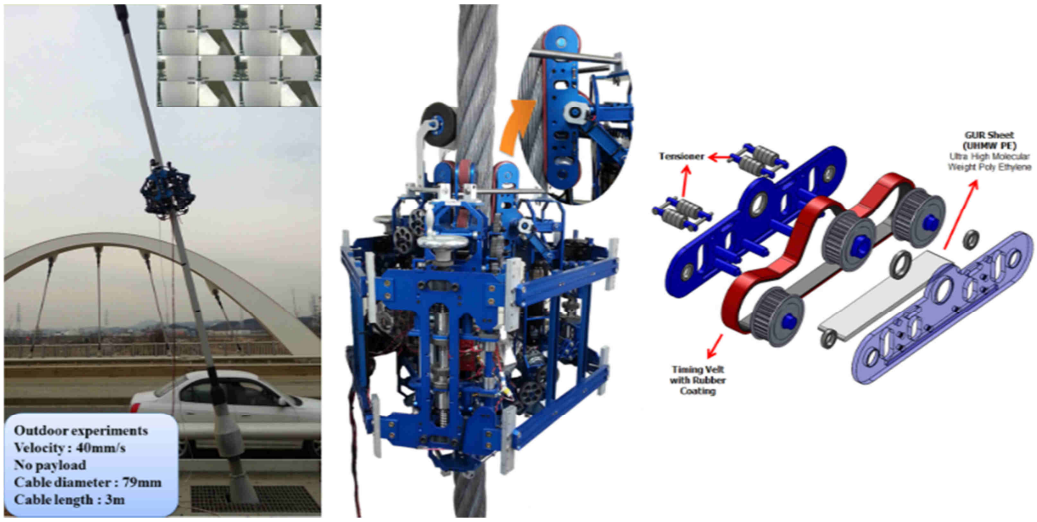

Figure 11: Cable based climbing robots [5]

Robots designed for moving on poles of construction sites, scaffolds. On the left of Figure 12 is the HyDRAS serpentine robot prototype climbs a pole by converting the oscillating motion of its joints to a whole body rolling motion, making it useful for construction inspection tasks [9]. On the right of figure 5 is the CIRCA (Climbing Inspection Robot with Compressed Air) is a concept of a robot using air muscles to climb scaffolding structures for inspection tasks. By connecting multiple modules together in different shapes, you achieve different methods of locomotion [10]

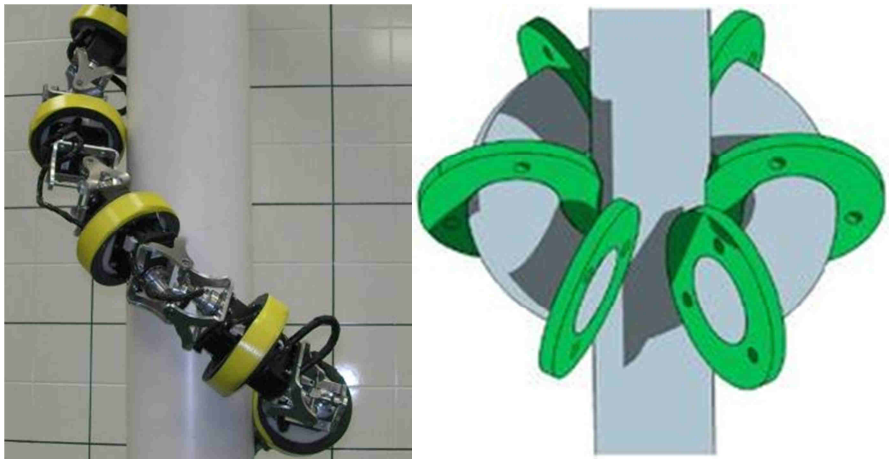

Figure 12: Pole climbing robots

Wall Climbing Robots designed to climb flat vertical surfaces using magnetic properties, top left Figure 13 shows a Prototype of Wall Climbing Robot for Tank Inspection, top right a magnetic crawler for inspection of large cargo holds and large tanks. Light-weight system using magnetic wheels (including hybrid leg-wheels) and a passive magnetic tail can climb tall metallic walls and overcome small obstacles [12]. On bottom left is the MicroMag™ mobile robotic inspection vehicle a compact, waterproof and magnetic unit equipped with an earth magnet component and vision systems [13]. Finally on the lower right is a weld inspection robot with magnetic adhesion [14].

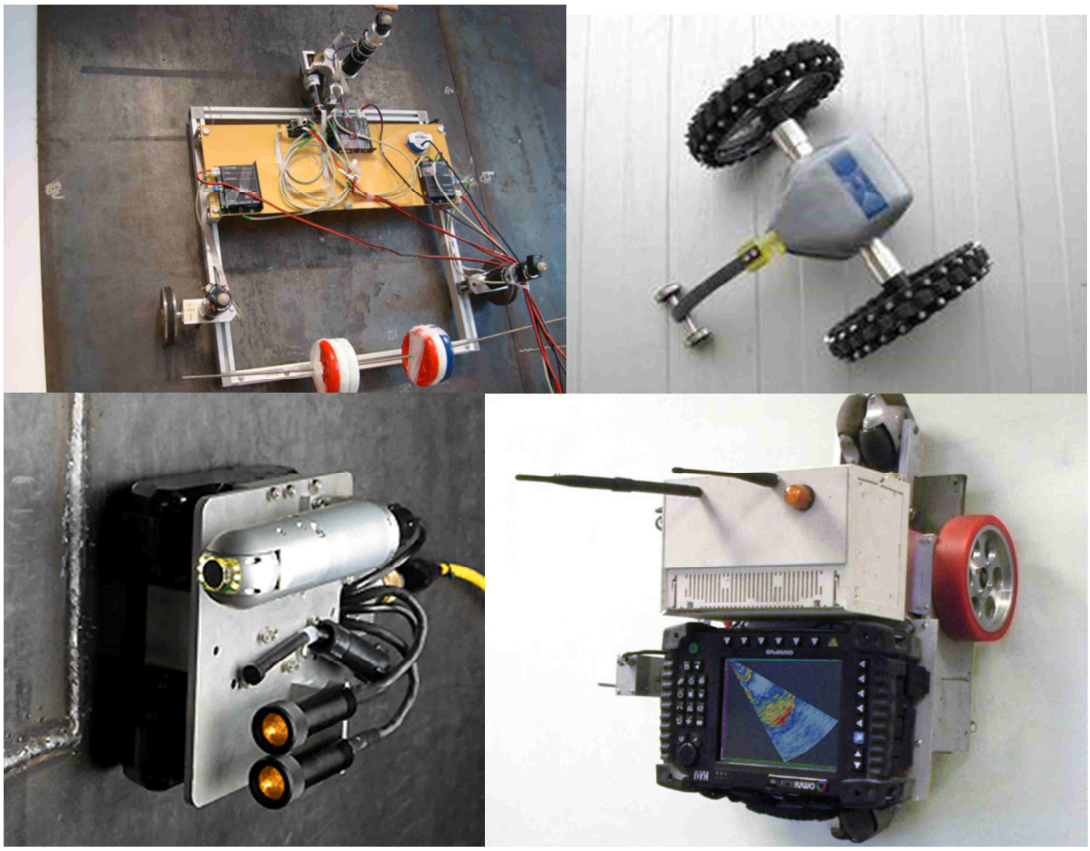

Figure 13: Climbing robots using magnetic adhesion mechanism

Climbing robots using electro-adhesion technology to enable wall climbing, in Figure 14 on the left is a Surface- and wall-climbing robot prototypes for surveillance, inspection, and sensor placement applications including remote surveillance or inspection of concrete pillars or other structures (such as bridges and tunnels) [15]. On the right is a multiple surface adhesion robot for visual inspection [16].

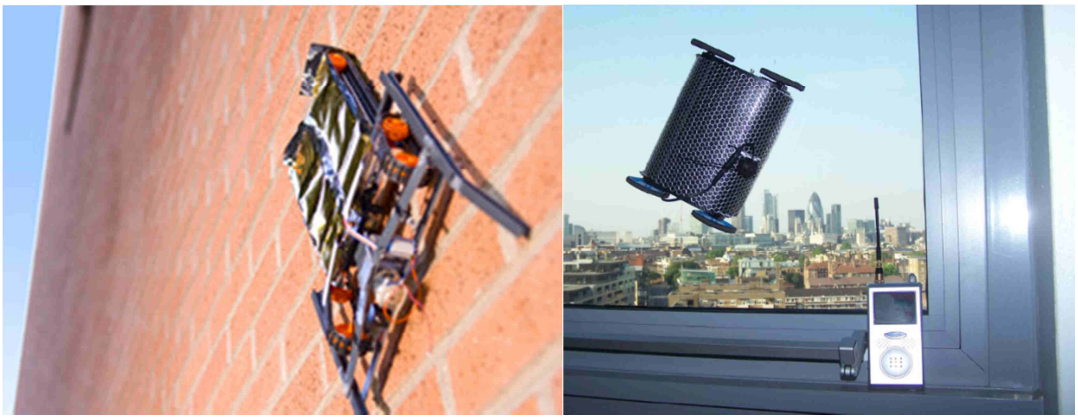

Figure 14: Climbing robots using electro-adhesive adhesion mechanism

Illustrated on the left in Figure 15 is a climbing robot for regular inspections of reinforced concrete structures. It generates the suction by creating a vortex “like a mini tornado” in a central tube. Only the wheels need to be in contact with the climbing surface [17]. Shown on the right is an ICM climber, a small, remote-controlled, lightweight climbing machine. The robot can climb walls, ceilings or rounded

surfaces. Held to the surface by vacuum force (patented, highly flexible seal), the machines adheres to hard surfaces: metal, concrete, brick, etc. [18].

Figure 15: Climbing robots using vacuum adhesion mechanism

MAINBOT project uses a vertical platform, see figure 16, to perform the following inspection activities:

Figure 16: MAINBOT climbing robot

- Surface defects detection in vertical structures. In CR plants a receiver located at the top of a tower heats molten salts. Receiver pipes have an external coating in order to improve radiation absorption. This coating has a thickness of microns. The climbing robot moves on

top of those panels performing eddy current inspection, to assess the status of the coating by measuring its thickness. Moreover, a visual camera records external surface to detect loss of coating.

- Internal defects detection. Detection of corrosion and internal defects in general (cracks, etc.) is required in many components in a power plant. The climbing robot can test the presence of this kind of possible defects in the collector tubes.

3.2.1.2 Ground inspection robots

Several wheeled robot platforms have been developed for general purpose and some of them are commercially available products. Here a short review of some robots designed for inspection is presented. The MIMROex robot developed by Fraunhofer [19] in 2009 is the first prototype of an offshore inspection robot that is capable of safely performing inspection and maintenance tasks, shown on the left in Figure 17. On the right the sensabot Inspection Robot developed by the group NREC/CMU [20] in 2012 is able to safely and cost-effectively inspect and monitor hazardous and remote production facilities

Figure 17: Ground based inspection robots (1) - MIMROex and sensabot Inspection Robot

In Figure 18 (left) is shown the robuCARTT from Robosoft [21] a general purpose Outdoor platform, used as a base platform in the Mainbot project. The specification is a 300 kg payload, 4 driving/steering wheels, speeds up to 18 km/h and a customizable configuration. On the right is the GUARDIAN robot from Robotnik [22] with a 100 kg payload, 2 driving/steering wheels, speed up to 3m/s and customizable (a wide range of robotics modules are available to easily extend its capabilities including vision, navigation, and localization systems).

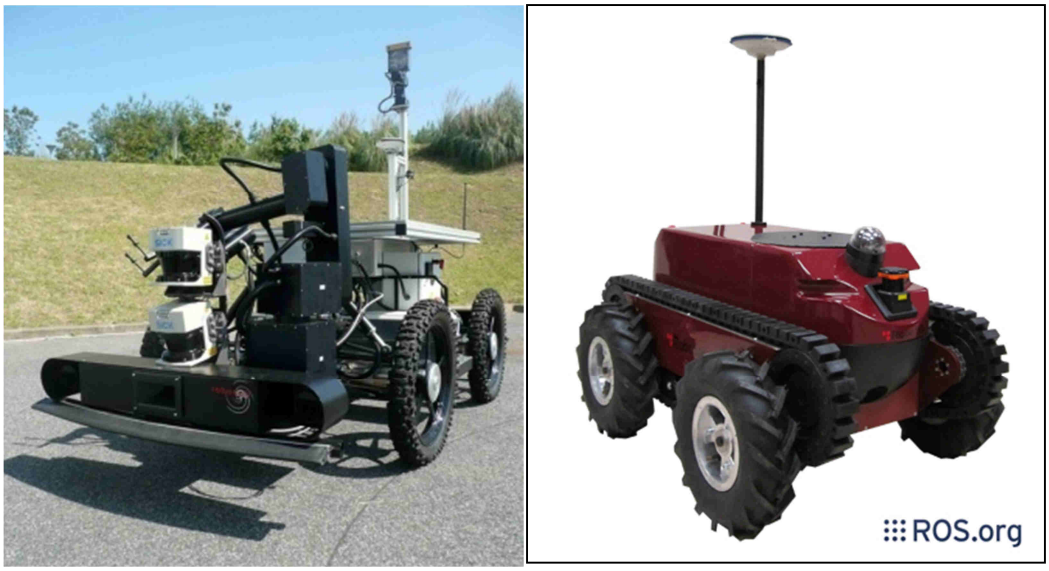

Figure 18: Ground based inspection robots (2) – RobuCARTT and GUARDIAN robot

On the left is Figure 19 the Quince [20] developed by Chiba Institute of Technology Japan in 2011 after the Fukushima accident for surveillance in the reactor buildings. Quince accomplished multiple missions in the buildings. The robot moves on five caterpillar-like crawlers via remote control. Its main body measures 66cm long and 48 cm wide. Next to this on the right is the PackBot [24] robot developed by iRobot in 2001 to inspect the World Trade Centre after the September 11 terrorist attacks. It was also used in Fukushima after the accident to inspect some buildings. Now iRobot has a complete line dedicated for inspection, security and defence.

Figure 19: Ground based inspection robots (3) – Quince and PackBot robot

The SCITOS G5 Manipulator from METRALAB [22], shown on the left in Figure 20 is equipped with Shunk Manipulator perfect for precise transportation needs. With the robotic arm the robot is able to transport fragile objects to specific locations with an astonishing accuracy of 2-3 cm. On the right is the Pioneer LX Research Platform from Adept [26], the indoor Pioneer LX is an advanced mobile robotics research platform based on the Adept Lynx industrial AIV (Autonomous Indoor Vehicle).

Figure 20: Ground based inspection robots (4) - SCITOS G5 Manipulator and Pioneer LX Research Platform

The MAINBOT project uses a ground platform composed of two main elements: a wheeled robot based on the robucarTT platform and a 6 DoF robuArm robotic arm mounted on it, see Figure 21.

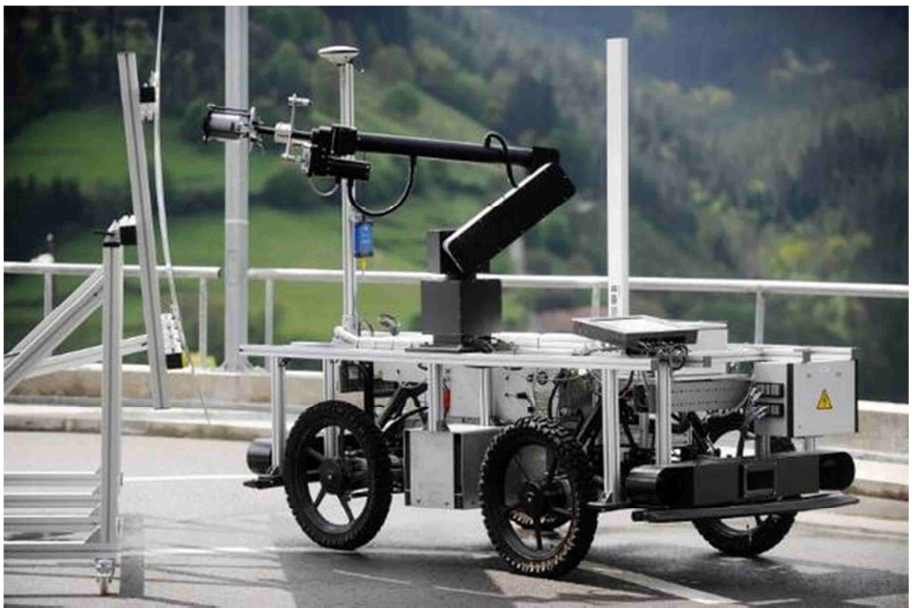

Figure 21: MAINBOT Ground robot

Based on the selection criteria (positive impact in plant, novelty, feasibility, risk) several operations to be performed autonomously by the robots were selected.

- Ubiquitous sensing - Measurement of reflectivity is done manually by operators using a special purpose sensor, the reflectometer.
- Leakage detection - Robots using thermography inspection techniques can perform this detection.
- Surface defects detection in horizontal structures - It is estimated that 2% of the mirrors must be replaced every year, and 0,83% mirrors are permanently broken in the plant. Ground robots in the plant look for broken mirrors since early detection can contribute to improve this efficiency. In addition, the ground robot patrolling at night and using thermography inspection can be used to identify any kind of loss of vacuum in receiver tubes.

References

[1] King, P., Comley, P., & Sansom, C. (2014). Parabolic Trough Surface form Mapping Using Photogrammetry and its Validation with a Large Coordinate Measuring Machine. Energy Procedia, 49, 118-125

[2] Montecchi et al., SolarPACES 2010

[3] K Montecchi et al., SolarPACES 2011

[4] NDT Encyclopedia,» [En línea]. Available: http://www.ndt.net/ndtaz/ndtaz.php.

[5] Sentinel NDT, [En línea]. Available: http://sentinel.thomasnet.com/category/pipeline-crawler-systems?.

[6] SAUL, [En línea]. Available: http://www.compositesworld.com/articles/nondestructive-inspection-better-faster-and-cheaper.

[7] Ultrasonic Inspection Robot “Pig“, [En línea]. Available: http://www.ipe.kit.edu/english/157.php.

[8] K. Intelligent Robotics and Mechatronic Systems Laboratory (IRMS), «Intelligent Robotics and Mechatronic Systems Laboratory (IRMS), Korea,» [En línea]. Available: http://mecha.skku.ac.kr/board/list.php?bbs_id=Robotics_12.

[9] U. Virginia Tech University, Virginia Tech University, US, [En línea]. Available: http://www.theepochtimes.com/n2/technology/three-pole-climbing-robots-designed-to-inspect-underwater-bridge-piers-8769.html.

[10] L. A. (. U. The Robotics & Mechanisms Laboratory (RoMeLa) at (University of California, «The Robotics & Mechanisms Laboratory (RoMeLa) at (University of California, Los Angeles (UCLA), USA,» [En línea]. Available:http://www.romela.org/main/CIRCA: Climbing Inspection Robot with Compressed Air.

[11] E. y. A. I. I. C. R. U. S. Dep. de Ingeniería Eléctrica, «Dep. de Ingeniería Eléctrica, Electrónica y Automática,E.T.S. Ingenieros Industriales Ciudad Real, UCLM, SPAIN,» [En línea]. Available: http://ieeexplore.ieee.org/stamp/stamp.jsp?tp=&arnumber=5675473.

[12] G. DFKI Bremen, «DFKI Bremen, Germany,» [En línea]. Available: http://robotik.dfki-bremen.de/en/research/robot-systems/magnet-crawler.html.

[13] N. B. C. C. Inuktun Services Ltd, «Inuktun Services Ltd, Nanaimo, British Columbia, CA,» [En línea]. Available: http://www.inuktun.com/crawler-vehicles/versatrax-100-micromag.html.

[14] «Weld magnetic robot,» [En línea]. Available: http://ieeexplore.ieee.org/stamp/stamp.jsp?tp=&arnumber=6695604.

[15] U. SRI International, «SRI International, US,» [En línea]. Available: http://www.sri.com/engage/products-solutions/electroadhesive-surface-climbing-robots#sthash.ShITsH0P.dpuf.

[16] M. s. ashesion, «Multiple surface adhesion,» [En línea]. Available:

http://ieeexplore.ieee.org/stamp/stamp.jsp?tp=&arnumber=6695604.

[17] S. ETH Zürich, «ETH Zürich, Switzerland,» [En línea]. Available: http://www.ifb.ethz.ch/corrosion/research/Robot.

[18] N. U. ICM - International Climbing Machines, «ICM - International Climbing Machines, NY USA,» [En línea]. Available: http://www.icm.cc/.

[19] B. a. P. K. a. S. H. Graf, «Mobile Robots for Offshore Inspection and Manipulation,» de IEEE/RSJ International Conference on Intelligent Robots and Systems, 2009.

[20] Sensabot, «Sensabot,» [En línea]. Available: http://www.rec.ri.cmu.edu/projects/shell/.

[21] RobucarTT Robosoft,» [En línea].

[22] Robotnik, Guardian, [En línea]. Available: http://robotnik.es/ilsupload/Robotnik_Guardian-e.pdf.«Quince, [En línea]. Available: http://www.jsme.or.jp/English/awards/awardn12-2.pdf.

[23] iRobot, [En línea]. Available: http://www.irobot.com/us/learn/defense/packbot.aspx.

[24] Metralab, [En línea]. Available: The SCITOS G5 Manipulator from METRALAB.

[25] Adept, Pioneer LX Research Platform from Adept, [En línea]. Available: http://www.mobilerobots.com/ResearchRobots/PioneerLX.aspx. [Último acceso: 2014].

[26] M. I. Solihin, Wahyudi y A. Legowo, «Fuzzy-tuned PID Anti-swing Control of Automatic Gantry Crane,» JOURNAL OF VIBRATION AND CONTROL, vol. 16, nº 1, pp. 127-145, 2010.

[27] M.-S. Park, D. Chwa y S.-K. Hong, «Antisway Tracking Control of Overhead Cranes With System Uncertainty and Actuator Nonlinearity Using an Adaptive Fuzzy Sliding-Mode Control,» IEEE TRANSACTIONS ON INDUSTRIAL ELECTRONICS, vol. 55, nº 11, pp. 3972-3984, 2008.

[28] M. B. Trabia, J. M. Renno y K. A. F. Moustafa, Generalized design of an anti-swing fuzzy logic controller for an overhead crane with hoist, JOURNAL OF VIBRATION AND CONTROL, vol. 14, nº 3, pp. 319-346, 2008.

[29] C.-Y. Chang y H. W. Lie, Real-Time Visual Tracking and Measurement to Control Fast Dynamics of Overhead Cranes, IEEE TRANSACTIONS ON INDUSTRIAL ELECTRONICS, vol. 59, nº 3, pp. 1640-1649, 2012.

[30] P. Hyla, Stereovision system for overhead travelling crane workspace visualization - validation approach, 2013 18TH INTERNATIONAL CONFERENCE ON METHODS AND MODELS IN AUTOMATION AND ROBOTICS (MMAR), pp. 69-74, 2013.

[31] P. Hyla y J. Szpytko, Vision Method for Rope Angle Swing Measurement for Overhead Travelling Cranes - Validation Approach, ACTIVITIES OF TRANSPORT TELEMATICS, vol. 395, pp. 370-377, 2013.

[32] Y. Fang, B. Ma, P. Wang y X. Zhang, «A Motion Planning-Based Adaptive Control Method for an Underactuated Crane System,» IEEE TRANSACTIONS ON CONTROL SYSTEMS TECHNOLOGY, vol. 20, nº 1, pp. 241-248, 2012.

[33] X. Zhang, Y. Fang y N. Sun, Minimum-Time Trajectory Planning for Underactuated Overhead Crane Systems With State and Control Constraints, IEEE TRANSACTIONS ON INDUSTRIAL ELECTRONICS, vol. 61, nº 12, pp. 6915-6925, 2014.

[34] N. Sun y Y. Fang, An efficient online trajectory generating method for underactuatedcrane systems, INTERNATIONAL JOURNAL OF ROBUST AND NONLINEAR CONTROL, vol. 24, nº 11, pp. 1653-1663, 2014.

[35] A. Kaneshige, Y. Kawasaki, S. Ueki y S. Nagai, Development of an Autonomous Mobile Overhead Traveling Crane with on-line Obstacle Recognition and Path-Planning Based on Obstacle Information -The Design of a Transfer Control System in Consideration of Oscillating Control, PROCEEDINGS OF THE 2ND INTERNATIONAL SYMPOSIUM ON COMPUTER, COMMUNICATION, CONTROL AND AUTOMATION, vol. 68, pp. 468-473, 2013.

[36] Interfaces and Control Systems for intuitive crane control, [En línea]. Available: https://smartech.gatech.edu/bitstream/handle/1853/31782/peng_chen_chih_200912_mast.pdf?sequence=1.

[37] Human Operator Studies of Portable Touchscreen Crane Control Interfaces.

[38] OctoMap An Efficient Probabilistic 3D Mapping Framework Based on Octrees, [En línea]. Available: http://octomap.github.io/.

[39] R. a. N. N. Fikes, STRIPS: A New Approach to the Application of Theorem Proving to Problem Solving, Artificial Intelligence, Vol. 2, 1971.

[40] R. Brooks, A robust layered control system for a mobile robot, IEEE J. Rob. Automation Vol. 2, 1986.

[41] J. C. A. P. D. B. E. F. a. J. B. Manuela Veloso, Integrating planning and learning: The PRODIGY architecture, Journal of Experimental and Theoretical AI, p. 7:81–120, 1995.

[42] A. L. B. a. M. L. Furst, Fast planning through planning graph analysis, de Proceedings of the 14th International Joint Conference, Montreal, 1995.

[43] L. K. a. T. Lozano-Perez, Unifying Perception, Estimation and Action for Mobile Manipulation via Belief Space Planning, de IEEE International Conference on Robotics and Automation, 2012.

[44] J. M. B. a. R. S. Wolfe, Combined Task and Motion Planning for Mobile Manipulation, de International Conference on Automated Planning and Scheduling, Toronto, Canada, 2010.

[45] E. McGann, Model-based, Hierarchical Control of a Mobile Manipulation Platform, de ICAPS Workshop on Planning and Plan Execution for Real-World Systems, Thessaloniki, Greece, 2009.

[46] Robot Web Tool, 2013. [En línea]. Available: http://robotwebtools.org/.

[47] K. Intelligent Robotics and Mechatronic Systems Laboratory (IRMS). [En línea]. Available: http://mecha.skku.ac.kr/board/list.php?bbs_id=Robotics_12.

[48] P. Debenest, M. Guarnieri, K. Takita, E. Fukushima, S. Hirose, K. Tamura, A. Kimura, H.

Kubokawa, N. Iwama, F. Shiga, Y. Morimura y Y. E. Ichioka, «Toward a Practical Robot for Inspection of High-Voltage Lines,» In proceeding of Field and Service Robotics (FSR), pp. 45-55, 2009.

[49] J. Lee, B. Cho, K. Jang, S. Jung, K. Oh, J. Park y J. Kim, «Development of Autonomous Cable Inspection Robot for Nuclear Power Plant,» In WASET, pp. 314-318, 2010.

[50] B. Luk, A. Collie, D. Cooke y S. Chen, «Walking and climbing service robots for safety inspection of nuclear reactor pressure vessels,» In Asia Pacific Conference on Risk Management and Safety , pp. 432-438, 2005.

[51] U. SRI International, «SRI International, US,» [En línea].

[52] D. C. Z. Dr D G Robertson, «Survey of Advanced Inspection Techniques & Recommendations for Best Practices,» European Technology Development Ltd - UK, 2008.

[53] Institute of Physical research and technology, [En línea]. Available: http://www.iprt.iastate.edu/assistance/nde/tools/radiographic

[54] I. Maurtua, L. Susperregui, A. Ansuategui, A. Fernández, A. Ibarguren, J. Molina, C. Tubio, C. Villasante, T. Felsch, C. Pérez, J.R. Rodríguez, M. Ghrissi. Non-destructive inspection in industrial equipment using robotic mobile manipulation. 21st SolarPACES Conference, Cape Town (South Africa), October 2015.

List of abbreviations and definitions

AIV	Autonomous Indoor Vehicle
CAA	Civil Aviation Authority
CIRCA	Climbing Inspection Robot with Compressed Air
CSP	Concentrated Solar Power
DoW	Description of Work
DSLR	Digital Single Lens Reflex
GPS	Global Positioning System
IAV	Intelligent Autonomous Vehicle
IR	Infrared
ITR	Inspection Receiver Tubes system
NDT	Non Destructive Testing
RTK	Real Time Kinetic
UAV	Unmanned Aerial Vehicle
UGR	Unmanned Ground Robot
UK	United Kingdom
WP	Work Package
VIS	Visual Inspection System methodology